ADVANCED INTELLIGENT SYSTEMS
Open Access
www.advintellsyst.com

Development of a Chemically Driven Biomimetic Modular Artificial Muscle (BiMAM)

*Pritish Nagwade, Minseok Kang, Jaeu Park, Jinwoong Jeong, Heejae Shin, Youngjun Cho, and Sanghoon Lee**

Human skeletal muscle is widely considered to be the most efficient actuator, leading to extensive research on developing artificial muscles. Bioinspired technologies such as soft robotics and biomimetics are used to produce artificial muscles with performance characteristics similar to those of their biological counterpart. Despite the complexity of human skeletal muscle, advanced engineering materials and unique approaches can help develop an artificial muscle that replicates its kinematic motions. Herein, biomimetic modular artificial muscle (BiMAM), which is the culmination of different design strategies, is presented, and fabrication methods aimed at developing this BiMAM. This chemically driven modular artificial muscle uses shape memory alloy coated with nanomaterials and nano-catalysts. Herein, a high-energy density fuel is employed to actuate this artificial muscle, enabling fast and efficient outputs. Multiple performance characteristics are determined by conducting controlled experiments. Various methods are demonstrated to control the fuel-based valve system and the actuation of the chemically driven artificial muscle. Lastly, to evaluate its functionality, the curling movement of a robotic finger using BiMAM is demonstrated.

1. Introduction

Skeletal muscles are complex structures that operate synergistically to produce movement, and their function has been extensively studied in engineering fields for the purpose of mimicking it.[1–3] Accordingly, researchers worldwide have developed artificial muscles that mimic the biological system as actuators to achieve capabilities comparable to natural muscles.[4–7] Various approaches have been taken to develop artificial muscles over the past few decades.[8–18] For example, dielectric elastomer–based actuators (DEA) have exhibited the ability to provide large strokes along with moderate stress generation upon actuation.[19] Pneumatic artificial muscles have been enabled to replicate contractile motion similar to a human bicep, offering controllable speeds and high force-to-weight ratios.[20] Shape memory alloy (SMA) actuators, specifically nitinol (NiTi), have been widely exploited to achieve immense amounts of stress based on the principle of phase transition upon a change in temperature like Joule heating, thereby allowing for control over actuation using electric manipulation.[21] However, these aforementioned artificial muscle technologies also have their limitations. DEA dielectric elastomers easily break down and show uncertainty in production, pneumatic artificial muscles require pressurized fluids and reservoirs, and SMA suffers from small contractions (4%≈8% strains) and limited bandwidth.[22] Since SMA suffers from issues like small contractions, it has not been proven to be useful in certain applications where larger actuation strokes might be needed.

Although materials such as SMA have their limitations, an innovative design approach can open up a realm of possibilities that cannot exist if SMA is used in a conventional manner. An example of such an approach is demonstrated by a hydrogel–matrix encapsulated NiTi actuator, which utilizes a different configuration of SMA wire to achieve a larger stroke.[23] However, the mentioned work relies on Joule heating for actuating the artificial muscle. While Joule heating is the most commonly used technique for actuating NiTi, it becomes unsuitable when such a design is scaled down in size. Also, Joule heating involves electrical wiring of multiple small actuating elements, introducing bulkiness, and intricacies to the system. Therefore, chemical-based actuation, such as catalytic combustion-based heating, has been demonstrated as an alternative to eliminate the need for electric energy.[24] RoBeetle, an untethered centimeter-scale robotic insect, successfully demonstrated mobility with onboard catalytic combustion-based closed-loop actuation and control mechanisms.[25] However, precise control of its locomotion and SMA heating/actuation is limited, as it was designed for an autonomous battery-free operation based on an electronic-free mechanical control mechanism of catalytic heating.

The concept of electromechanically controlling the catalytic heating of SMA has been previously discussed.[26]

P. Nagwade, M. Kang, J. Park, J. Jeong, H. Shin, Y. Cho, S. Lee
Department of Robotics and Mechatronics
DGIST
Daegu 42988, Republic of Korea
E-mail: hoonw@dgist.ac.kr

The ORCID identification number(s) for the author(s) of this article can be found under https://doi.org/10.1002/aisy.202300200.

DOI: 10.1002/aisy.202300200

Nevertheless, the development of a modular artificial muscle equipped with catalyst-coated SMA, an electromechanical valve system, and a chemical-fuel tank has not been reported. Drawing inspiration from the contractile elements of skeletal muscle, various principles from this biological counterpart can be applied when developing a complete modular artificial muscle.

Bioinspired designs have continuously demonstrated advantages over conventional approaches in the field of robotics.[27–32] For instance, a bioinspired single-fiber actuator comprising advanced engineering materials like graphene and liquid crystal elastomers showed remarkable biomimicry of skeletal muscle.[33] While this light- and photothermal-actuated artificial muscles surpass the performance of other liquid crystal elastomer–based actuators, it is important to consider the convergence of artificial muscles and humans to validate a complete bioinspired approach.

Several crucial aspects need to be considered in the subsequent stages of development. First, the energy source is a crucial factor in modular artificial muscle. The catalytic-combustion method allows for heat generation using various high-energy density chemicals, such as hydrogen (H_2), propane (C_3H_8), and methanol (CH_3OH) for fuels. Chemical-based heating also enables efficient driving of multiple SMA wires simultaneously. Second, the proposed artificial muscle technology should possess the flexibility to adjust its modular functions according to the application's requirements. Unique design and fabrication techniques for artificial muscle units (AMUs) are necessary for application-dependent production to manipulate force or stroke parameters. Lastly, artificial muscles should ultimately be controlled by the user's intention based on biological information, such as muscle or neural signals. Surface electromyography (sEMG) signals are widely utilized in robots, exosuits, and bionic prosthetics to establish biopotential signal-based control. To control a chemically driven artificial muscle using such neural signals, an electromechanical valve system is necessary.

With this understanding, we developed biomimetic modular artificial muscle (BiMAM), which was chemically powered and could be bio-electrically triggered. In this work, we utilized methanol as a fuel due to its ability to remain in the liquid state at atmospheric pressure and evaporate at room temperature. This property facilitated easier storage and enables natural fuel transport. We investigated a catalytic combustion-based heating technique where the actuating element is dip-coated with carbon nanotubes (CNTs) and platinum black (Pt black).

Our novel design and fabrication methods enable adaptive configurations based on the desired application. For example, in applications requiring more force generation, multiple NiTi wires can be placed within a single AMU. For applications requiring larger strokes, two or more AMUs can be placed in series to increase the overall stroke length. Furthermore, we designed a centimeter-scale electromechanical valve system that operates using the principles of electromagnetism to open the valve and actuate the AMU. We utilized surface-mount device electronics to adequately energize this valve system and enable control via the general-purpose input–output (GPIO) pins of any microcontroller board. This inclusion of an electromechanical valve system allows for sEMG signal-based triggering of BiMAM. With the use of this near-biomechatronic technology, we finally showcase its application by moving an in-house 3D-printed robotic finger.

To the best of our knowledge, this is the first demonstration of an sEMG-triggered actuation of a chemically driven modular artificial muscle for the movement of a robotic finger.

2. Results and Discussion

2.1. Design and Fabrication of AMU

The proposed BiMAM comprises two main components: the AMU and the modular element. The conceptual idea is represented in **Figure 1**a and the biomimetic design is shown in Figure 1b. The AMU, illustrated in Figure 1c, is the main actuating element consisting of NiTi wires held in place by a hard polymer base. When subjected to external force, NiTi wires deform and can be brought back to their original state by applying heat. During this process, they produce a large force but exhibit small strokes of up to 4%–8% of their total length. However, the biomimetic-bending-type configuration in Figure 1d allows for a significantly larger available stroke compared to the conventional straight configuration of NiTi wires.

With the method described in Experimental Section, we estimate the actuation stroke length for the biomimetic configuration based on the strain and bend-diameter-related information provided by a manufacturer.[34] Based on the modeling estimations, an AMU equipped with a single 10 mm NiTi wire with a thickness of 0.25 mm can achieve a stroke of 34% of its original length while staying within the recommended outer-surface strain limit of 4%. Figure S1a, Supporting Information, shows the relationship between the bending diameter and outer-surface strain of a 1 mm NiTi wire. Figure S1b, Supporting Information, shows the bending diameter values and the strains occurring on the outer surface. Figure S1c, Supporting Information, shows the estimated strokes for 12 mm NiTi-wired AMU through 3D modeling. The estimated values for outer-surface strains up to 4% are listed in Table S1, Supporting Information. Theoretically, a longer NiTi wire will result in longer strokes. However, the increased length of the NiTi wire in such a configuration will affect the actuation force capability since the wire will have to pull its own weight after a certain point.

We developed an adaptive fabrication method that allowed for the free adjustment of the number of wires or wire placement patterns as desired. The fabrication process of the AMU is explained in the Experimental Section and schematically illustrated in Figure S2, Supporting Information. The base of the AMU is a UV-curable acrylate prepolymer, which must possess sufficient strength to withstand the force and heat during actuation. A tensile test experiment was performed on two 8 mm by 20 mm acrylate prepolymer bases with a thickness of 2 mm, as shown in Figure S3a, Supporting Information. This solid polymer base exhibited excellent performance under high stress as seen in Figure S3b, Supporting Information. Additionally, the base showed no structural changes when subjected to high temperatures (<150 °C) for several minutes. In theory, the actuation force of thin NiTi wires and the applied heat will not cause any mechanical or structural deformation to the base during operation. **Figure 2**a shows a fabricated AMU with multiple wires.

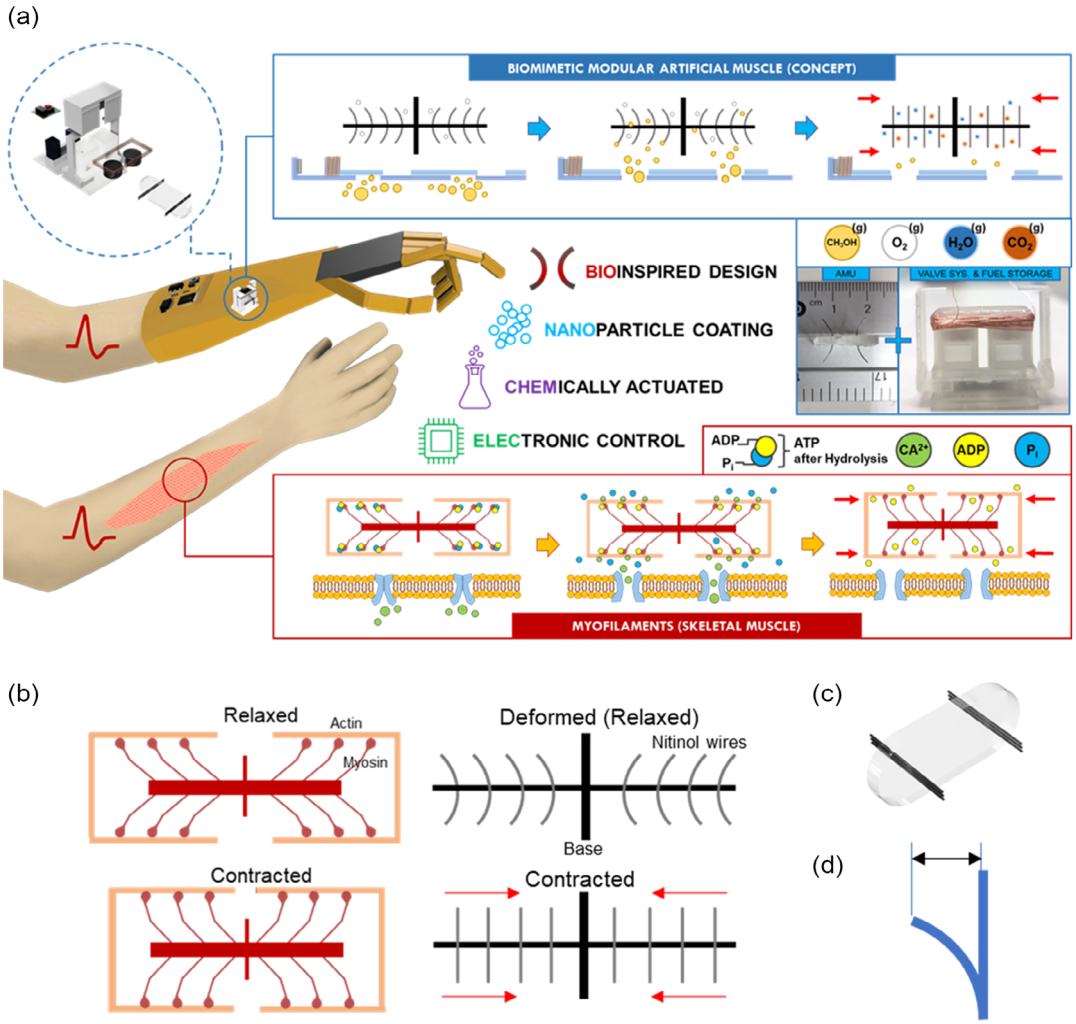

Figure 1. a) Conceptual illustration showcasing the bioinspired design. b) The 1D structural design similarities between the myofilaments of skeletal muscle and the artificial muscle unit (AMU). c) Conceptual 3D model of AMU. d) Graphic showing the adjusting-curve-type actuator stroke of a shape memory alloy (SMA) wire.

Figure 2b shows a single-NiTi wire AMU in the deformed and actuated state.

A NiTi wire can be actuated using heat produced from Joule heating, which allows easy electronic control over the actuation.[35] However, to actuate the multiple centimeter-scale NiTi wires in the AMU, complex electrical wiring and electronics systems would be required. Additionally, we consider the fact that using a battery to provide electric energy for Joule heating would increase the overall size of the modular artificial muscle. Chemical-based heating, such as catalytic combustion of fuel over a catalyst-coated NiTi wire, can eliminate the need for electrical wiring. Figure S4a,b, Supporting Information, illustrates how the catalytic combustion of methanol over platinum nanoparticles (Pt black) can be used for heating and actuating an SMA wire. Moreover, this method allows for the actuation of multiple centimeter-scale NiTi wires simultaneously. Due to methanol's ability to evaporate and catalytically combust on the surface of platinum nanoparticles at room temperature, it is a favorable option for the chemical-based heating of AMU. Methanol can also be stored in liquid form at atmospheric pressure, which is an important factor considering the modularity aspect of this work. Additionally, the byproducts of the catalytic reaction are unhazardous and in the gaseous state.

However, using chemical-based actuation restricts the electronic control of AMU's actuation. To overcome these limitations, we conceptualize an electromechanical valve system that can regulate the flow of chemical fumes to electrically trigger chemical-based actuation. Figure 2c shows our conceptual method for controlling the actuation of a chemically driven AMU.

To enable catalytic-combustion-based heating, we fabricated a CNT/Pt-hybrid NiTi wire as shown in **Figure 3**a,b. Since the speed of actuation is an important parameter for artificial muscles, we used a layer of CNTs to act as a thermal conductor for transferring the heating from Pt black to NiTi wires. CNTs are known to be excellent thermal conductors.[36] Platinum nanoparticles wrapped in short multiwalled carbon nanotubes

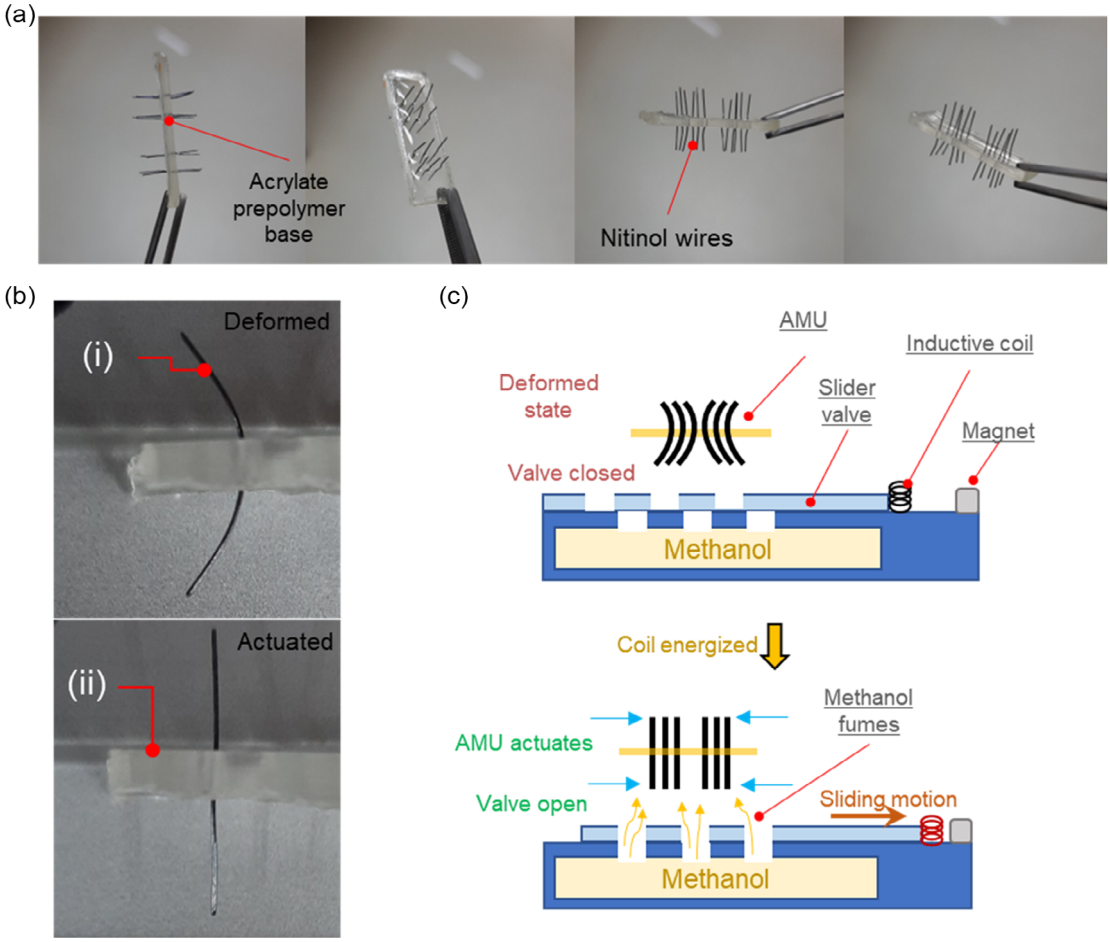

Figure 2. a) Fabricated AMU with multiple NiTi wires. b) Single-wire AMU in i) deformed state and ii) actuated state. c) Conceptual diagram of electronic control of actuating multi-wired AMU with chemical fuel (methanol).

(MWCNT) sheets have been used for hydrogen-based catalytic heating of SMA, demonstrating the material's advantages as a thermal conductor.[37] Thermal conductance of short-MWCNT and long-MWCNT has been measured in a polymer matrix, with long-MWCNT showing superiority in thermal conductance mainly due to its better percolation compared to short-MWCNT.[38] However, in this work, we directly attached the short-MWCNT particles to the NiTi wires to achieve maximum surface area contact between nanoparticles and SMA for faster thermal conduction. To coat the NiTi wires used in the AMU, we employed a dip-coating method to form ultrathin layers of CNT and platinum nanoparticles on the surface of NiTi wires.

The fabrication process of this CNT/Pt-hybrid NiTi wire is described in Experimental Section and Figure S5, Supporting Information, illustrates the process. Microscopic images of the surface of the SMA actuator are shown in Figure 3c. The average thickness of the CNT-coating is around 15 μm. The coating did not appear to impose any noticeable restriction to the bending of NiTi wire. The average thickness of Pt black–coating over the CNT layer is around 5 μm. A simple experiment determined that this CNT/Pt-hybrid NiTi wire actuates when exposed to methanol fumes. To further validate the use of CNT as a thermal-conductive material, we compared its catalytic-heating performance with that of a thermal-conductive paste. Figure S6, Supporting Information, indicates that CNT-coated catalytic heating showed stable actuation compared to the thermal paste. However, parameters, such as thermal paste layer thickness, environmental disturbances, and Pt black agglutination, play an important part in stable catalytic heating, and alternating these parameters can give various outcomes. We observed that increasing the catalyst loading on the NiTi wire caused Pt black to self-ignite and glow red (due to overheating), rendering the catalyst unresponsive to the methanol fuel. Additionally, overheating of the NiTi wire caused permanent damage. When the catalyst loading was reduced, we observed that the actuation was disoriented and slow, and in some cases completely unresponsive. Through trial and error, we established the optimal thickness of the Pt-coating layer for our work.

2.2. Catalytic-Heating Performance of Chemically Driven Single-Wire AMU

Before developing BiMAM, chemical-based actuation of the AMU was tested to obtain the parameters for designing the modular system. Particularly, we conducted experiments to

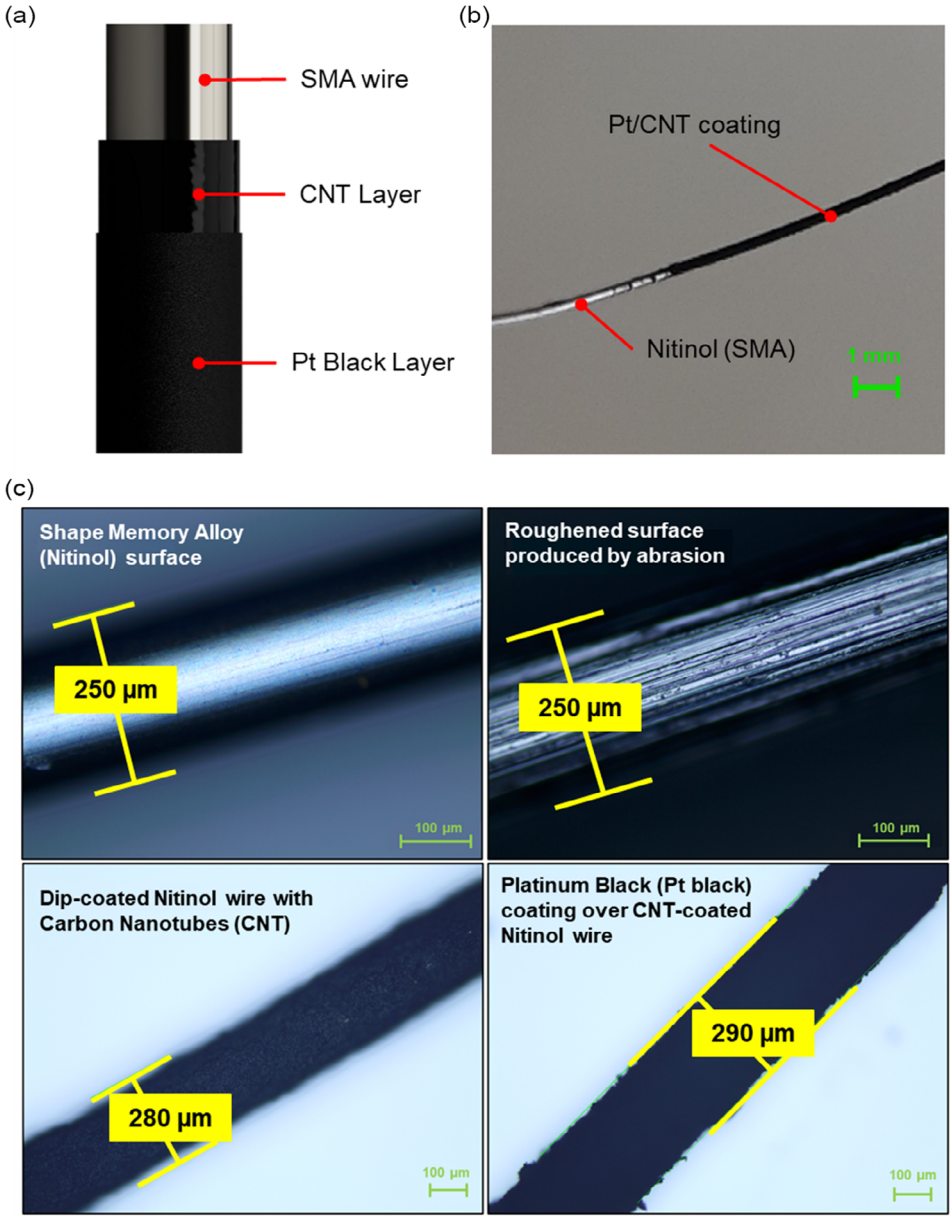

Figure 3. a) Illustration of different coating layers on SMA wire. b) Image of a carbon nanotubes (CNT)/Pt-coated NiTi wire. c) Microscopic imaging of the wires at different stages of the coating process.

determine characteristics like the response time of catalytic heating by exposing methanol fumes to Pt/CNT-coated temperature sensor, the effect of the gap between the methanol source and AMU on actuation, and the speed of actuation of AMU in response to valve operating time. A 250 µm thickness NiTi wire–based AMU is used for all experiments, unless otherwise specified.

The ratio of methanol–air–vapor/air mixture for steady-state catalytic combustion of methanol over Pt nanoparticles is <14.4%, which can be maintained at a thermal equilibrium for hours.[39] To increase the heating rate, the ratio should be greater than 14.4%. However, controlling these ratios without the involvement of precision systems is challenging. Since methanol fumes need to be directed toward the catalytic artificial muscle with a concentration higher than that 14.4%, it is necessary to ensure that the fumes are directed in a way that prevents scattering. The concentration of fumes is more likely to be higher near the surface of the fuel and tends to scatter as the distance from the fuel surface increases. An experiment was carried out to observe this phenomenon and validate the theory. The experimental setup is described in Experimental Section and Figure S7, Supporting Information. **Figure 4**a shows a plot comparing catalytic heating at different distances. It can be observed that at 2 and 4 mm distances, the temperature rise and fall have stability, indicating efficient catalytic heating. However, at a 6 mm distance, catalytic heating is slower and chaotic in nature.

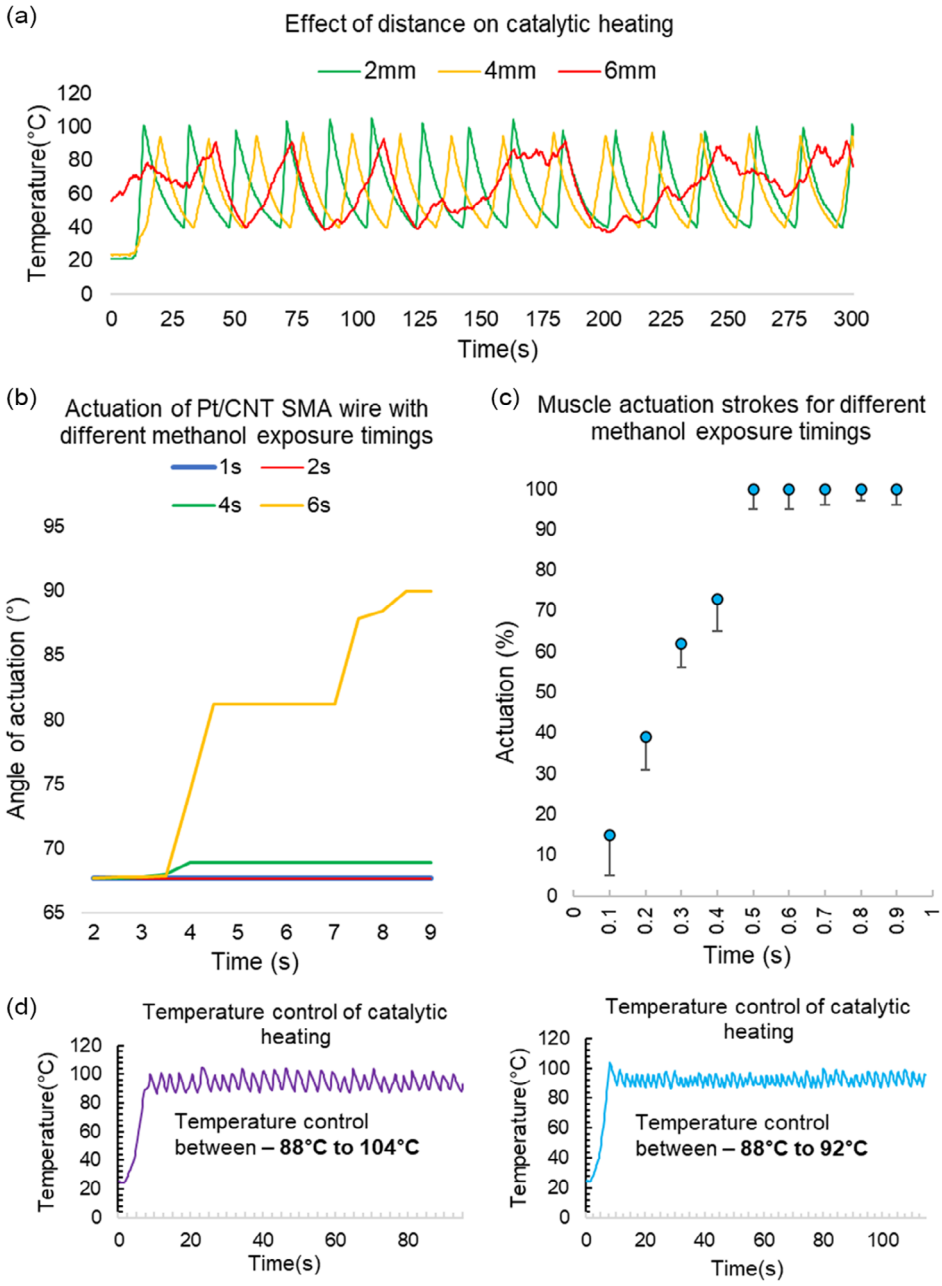

Figure 4. a) Plot showing the effect of distance on catalytic heating. b) Plot showing actuation attempts with different exposure timings with a 6 mm distance between the fuel source and catalyst-coated SMA. c) Plot showing actuation strokes for different exposure timings with a 2 mm distance between the fuel source and catalyst-coated SMA. d) Two plots showcasing temperature control ability for catalytic heating with programmable temperature limits with a 88–104 °C limit (left) and 88–92 °C limit (right).

Keeping a long distance between the Pt/CNT-coated sensor and the fuel source results in the fume taking more time to reach the sensor. Moreover, wider distances expose the fumes to environmental disturbances, causing more scattering and resulting in a lower concentration of methanol fumes over the muscle. Figure 4b shows how different exposure timings with a 6 mm distance between the fuel source and catalyst-coated SMA can affect actuation and Figure S8, Supporting Information, shows the experimental setup. Consequently, the catalytic heating becomes disoriented. The distance between the fuel source and catalytic muscle is an important factor to consider when designing the BiMAM since it can affect the concentration of fumes required to steady heat generation and actuation.

In this article, the speed of actuation is defined as the total time it takes for the AMU to completely actuate once the methanol fumes disperse. When a skeletal muscle actuates (contraction of muscle), which is biochemically driven, the speed of actuation includes the aftermath of a neural signal triggering the motor

synapse.[40] Adhering to that statement, the time taken for methanol fumes to make contact with the AMU is necessary to include as it is a part of the actuation process. To analyze the speed of actuation, AMU is exposed to methanol fumes for different durations ranging from 100 to 900 ms as seen in Movie S2, Supporting Information. The experimental setup is described in Experimental Section and Figure S9, Supporting Information. From the experimental data in Figure 4c and Table S2, Supporting Information, we can see that the time required to complete the actuation stroke is between 0.5 and 0.6 s. Shorter (incomplete) strokes are achieved when the time windows for the methanol fume to contact the Pt/CNT-coated NiTi wire are smaller, i.e., 0.1, 0.2, 0.3, and 0.4 s. When the valve is open for a smaller amount of time, the effective fume concentration needed for catalytic heating would not sustain for the time required for the Pt/CNT-coated NiTi wire to completely actuate, resulting in incomplete actuation. Complete actuation strokes can be seen beyond the 0.6 s window, such as 0.7, 0.8, and 0.9 s, but the issue of overheating can occur if catalytic heating sustains itself for longer periods. Figure 4d shows how this overheating issue can be counteracted. It is possible to control overheating by implementing a feedback loop that senses the temperature and keeps the methanol fume contact within a certain desired limit. Since the methanol fume contact is dependent on an electromechanical valve system, a fast ON/OFF trigger can maintain the concentration required for steady heating.

2.3. Performance and Application of Chemically Driven Single-Wire and Multi-Wire AMU

The performance of the fabricated muscle units is tested in terms of stroke (no-load and with bias weight), force generation, and bandwidth. Figure S10, Supporting Information, shows that the experimental stroke values, estimated stroke values through modeling, and corrected stroke values for a single AMU with two wires actuating in opposite directions and three similar AMUs actuating in series. The no-load stroke achieved by a single AMU with two wires actuating in opposite directions at 2% deformation is 4 mm. As anticipated, three AMUs connected in series achieve a three times larger stroke of 12 mm. However, the estimated stroke values from the modeling largely differed from the experimental values. Upon investigation, it was found that the modeling did not consider the hindrance caused by the 2 mm thick polymer base that holds the NiTi wires. After remodeling AMU with the polymer base's effect on the bending of NiTi wires, the estimated and recorded stroke values correspond with each other.

Figure 5a shows the cyclic operation of a 12 mm single-wire AMU subjected to a spring-bias force of 10 g at a 2 mm distance from its resting tip position. A single actuation cycle consists of actuation (heating) and deformation (cooling). This chemically driven AMU completes 11 cycles per minute (CPM), with a working frequency calculated to be 0.18 Hz. The experiment also demonstrated the robustness of AMU as it showed continuous operation for 100+ cycles with 2 mm average strokes for over 10 min as seen in Figure 5a. The experimental setup is shown in Figure S11a, Supporting Information, and schematically illustrated in Figure S11b, Supporting Information. During this experiment, we observed the CNT/Pt-coating on NiTi wire. The coating displayed complacent mechanical contact and no loose particles of the coating were detected. This cycling test provides us with an adequate indication that the CNT/Pt-coating can mechanically stay attached to the abrased surface of the NiTi wire for multiple actuation cycles. **Table 1** shows a comparison between AMU and other related works.

Figure 5c schematically illustrates the different positions of a NiTi wire when a bias weight is introduced against it before actuation. The actuation stroke length achieved by the single-, double-, and triple-wired AMU varies depending on the bias weight since it considers the initial deflection caused by the bias weight. It is also evident that as the number of NiTi wires in an AMU actuating in the same direction increases, the bias weight needs to considerably increase to deform (bend) the wires. Figure 5d schematically illustrates the actuation strokes achieved against the bias weights. It is important to note that even though the NiTi wires actuate upon being heated, they do not completely reach back to the "relaxed state" when heavier bias weights are introduced. All the deflection and stroke values were carefully measured using a digital vernier caliper. Figure 5e shows deflection in millimeters caused by the different weights attached to the AMUs with single, double, and triple NiTi wires. Figure 5f shows the actuation stroke achieved by AMUs with the single, double, and triple NiTi wires producing a pulling force in the same direction. Figure S12, Supporting Information, shows the experimental setup layout. Upon simple observation, we can see that introducing multiple wires to AMU that actuate in the same direction can achieve larger strokes and greater pull force, but require considerably larger bias weight initially. Longer strokes and greater pull force can thus be achieved with this biomimetic design of AMU, with one condition: considerable bias force will be required initially. The biomimetic adjusting-curvature-type actuation of AMU has the advantage of offering larger actuation strokes, but the actuation force that it can generate is compromised. We calculate the work output and maximum average power of AMU using Equation (1)

$$W_{\mathrm{AMU}} = Fd = mgd \tag{1}$$

After further modifying Equation (1) to include the varying force from the plastic film, we get

$$W_{\mathrm{AMU}} = \frac{1}{2}(m_{\mathrm{p}} - m_{\mathrm{z}})gd \tag{2}$$

where m_{p} is the average weight at 2 mm actuation stroke and m_{z} is the weight at a fully relaxed state. We measure the maximum average work output of the single-wired AMU to be 98.1 μJ at 0.18 Hz. From this experiment, the average power is calculated to be 17.64 μW when a varying spring load is applying an average force of 0.04905 N for an average displacement of 2 mm. However, if we consider the maximum load-carrying capacity of a single-wired AMU that we observed (64 g), and put it in Equation (1), we get the maximum average work output to be 226 mW assuming the same operating frequency of 0.18 Hz.

Additionally, to demonstrate the versatility of our fabrication techniques, we fabricated AMUs using different diameter SMA wires. NiTi wires of 125, 250, and 375 μm thickness were used to fabricate single-wired AMUs. Keeping all the actuation

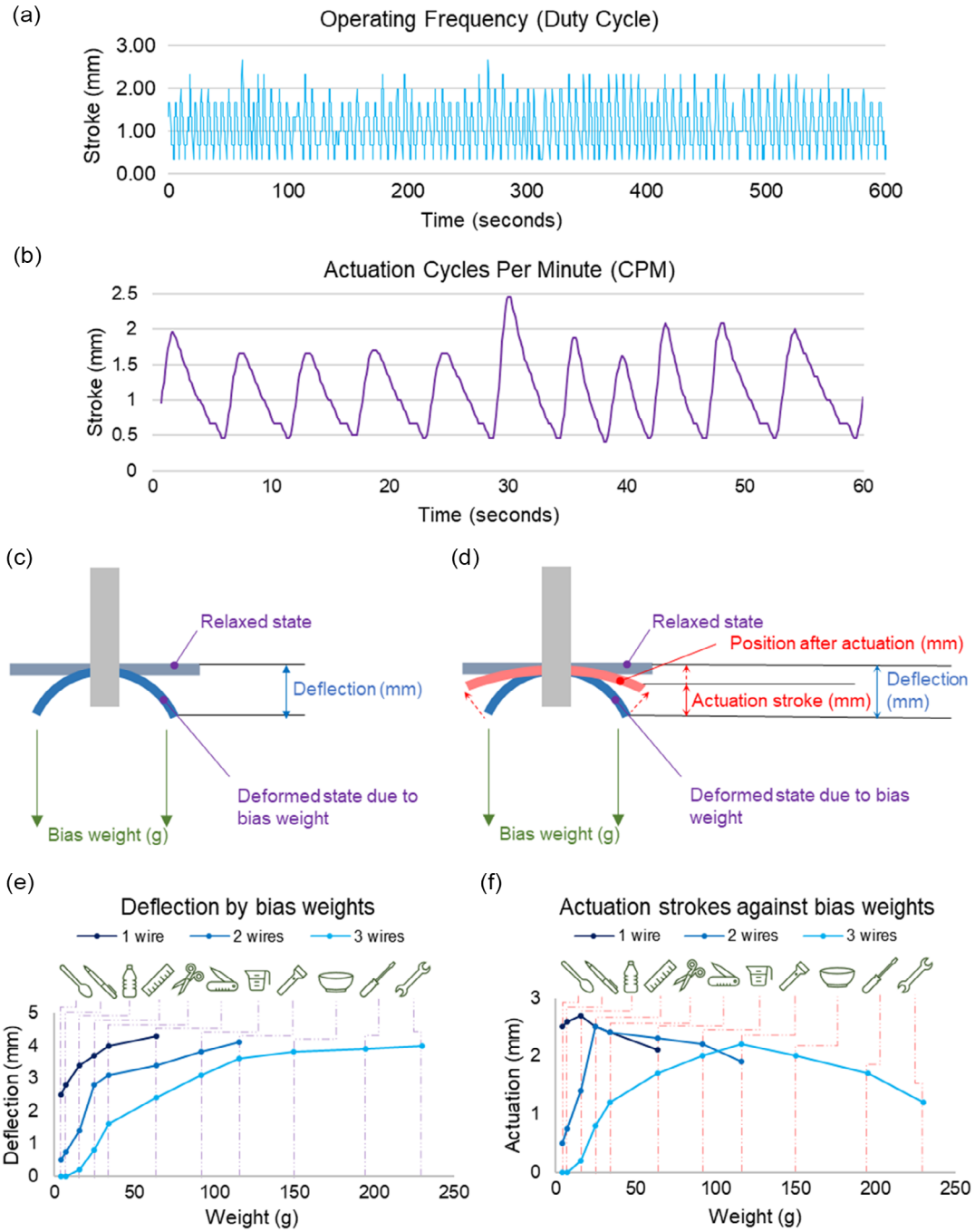

Figure 5. a) Plot showing the operating frequency of a single-wired AMU b) Plot showing actuation cycles per minute (CPM) of AMU. c) Schematic showing the positions of a NiTi wire when bias weights are introduced. d) Schematic showing positions of a NiTi wire after actuation against bias weights. e) Plot showing the deflection caused in 1-, 2-, and 3-wired AMUs due to different bias weights. f) Actuation strokes achieved against the bias weights by 1-, 2-, and 3-wired AMUs.

parameters the same during the catalytic heating of the three different thickness wires, we observed that the performance in terms of speed of actuation speed and stroke using catalytic actuation (Movie S4a, Supporting Information) is similar to that of direct heating–based actuation using a heat gun (Movie S4b, Supporting Information). Thicker NiTi wires require more time to actuate in both actuation methods. Figure S13, Supporting Information, shows the corresponding plot. The bending curvature is limited when using thicker wire; however, the actuation force generated by thicker NiTi wires is larger than thin wires. By employing the adaptive AMU fabrication method, actuation force and stroke values can be easily adjusted by integrating thicker or

Table 1. A comparison between the performances of similar works.

Muscle	Actuation–configuration	Actuation method	Energy source	Thermal conductor	Wire diameter [μm]	Wire length [mm]	Linear stroke [% of wire length]	Actuation time [s]	Relax. time [s]	Frequency [Hz]
HENA[23]	Adjusting curve	Joule heating	External DC supply	NA	250	40	35–62.5	≈2	≈3	0.2
RoBeetle[25]	Linear	Catalytic heating	Methanol	Thermal paste	50.8	9.8	≈1.2	<2	≈2	1
CC-engine[26]	Linear (leaf spring)	Catalytic heating	Hydrogen	Thermal paste	38.1	13	≈7	<1	<1	1–6
AMU (Our work)	Adjusting curve	Catalytic heating	Methanol	Carbon Nanotubes	250	12	15–25	≈0.5	≈4.5	0.18

thinner wires during fabrication, thus enabling application-focused fabrication.

Furthermore, to demonstrate the use of AMU in an untethered application, we designed and developed a simple inchworm robot that uses AMU for its movement (Figure S14a, Supporting Information). The inchworm was fabricated using 3D printing and a plastic sheet for the bending portion. The plastic sheet also provided an effective counterforce for the AMU to deform. To demonstrate the movement of the robotic inchworm, methanol fuel fumes were manually provided using a pair of tweezers and cotton infused with liquid methanol. When the muscle actuates, the flexible plastic sheet is forced to bend, causing the inchworm robot to contract its body. When the methanol exposure is paused, the AMU starts cooling down and starts deforming as the flexible plastic sheet forces itself to its original form, causing the inchworm robot to stretch its body. This cycle of contraction and relaxation propels the inchworm forward, producing movement. The locomotion of the inchworm resulting from this contraction–relaxation–actuation cycle is shown in Movie S4 and Figure S14b, Supporting Information.

2.4. Development and Characteristics of BiMAM

To demonstrate electronic control of chemically actuated AMU, we designed and developed BiMAM, an independent self-contained unit that included additional elements such as a fuel container, an electromechanical valve system, and an electronic triggering system to activate the fuel-valve system. **Figure 6**a shows BiMAM next to a coin for scaling reference. Figure 6b represents the 3D conceptual model that was carefully designed based on the experimentally gathered parameters of the chemically driven AMU.

The ability to be controlled by any commercially available microcontroller is of utmost importance to demonstrate its modularity. Essentially, a microcontroller acts as the brain of BiMAM. The fuel-valve system is designed using a 3D modeling software and printed using a Resin 3D printer (Formlabs Form3+) with clear resin as the material. The fuel-valve system is designed to securely hold the muscle unit in place, store methanol fuel, and integrate an electromagnetic system that provides us with an operating sliding valve mechanism. All the components of the modular artificial muscle are shown in Figure 6c. It consists of the AMU (acrylate prepolymer base, CNT/Pt-hybrid NiTi wires), copper coil (0.1 mm), neodymium magnets (6 pieces, 1 mm thickness, 6 mm diameter), a valve slider, muscle unit holder, fuel container, and electronics to provide required input to the copper coil. Figure S15, Supporting Information, shows the circuit diagram of the electronics used to energize the coil. It is similar to the electronics used to drive a commercial relay module using a development board such as an Arduino. The electrical components used are as follows: an negative-positive-negative (NPN) transistor (MMBT2222), a diode (IN4007), a resistor (150 ohms), and a status light emitting diode (LED). Note that in the fabricated model of BiMAM, the electronics are not embedded as per the conceptual design, but the components used are accurate to scale. Movie S5, Supporting Information, shows the basic working operation and actuation of BiMAM. The electric current drawn by the circuitry and the coil from the power supply pin of the Arduino was measured to be between 210 and 220 mA. The connection used as a trigger for opening and closing the valve draws an additional 10 mA. According to the datasheets of the NiTi wires provided by the manufacturer (Dynalloy Inc.), the electric current required to heat the 250 μm diameter wire is 1050 mA to achieve contraction in 1 s. BiMAM in comparison draws almost four times less current to achieve actuation for the same NiTi wire. For 150 and 375 μm NiTi wires, the current requirement stated in the datasheets by the manufacturer was 320 and 2250 mA, respectively, to achieve contraction in 1 s. For BiMAM, the change in NiTi wire diameter does not affect the current requirements since the actuation is chemically powered.

The fuel container has a total volume of 495 mm^2. The top half of the container is divided into two parts, each with a volume of 90 mm^2. The bottom half of the container has a volume of 315 mm^2. A total of 490 μL of liquid methanol can be stored inside this container. The average evaporation rate of methanol, when the valve is constantly in the open position, is 10.7 $\mu L\,min^{-1}$. Figure S16, Supporting Information, shows the methanol evaporation rate when the valve is in a continuous open. The rate of evaporation in the upper half of the container is comparatively faster than that of the lower half. This effect can simply be associated with the volume difference of the fuel and the relative distance of the fuel to the opening of the valve. The total time taken for the fuel to completely evaporate in a continuous open state was 45 min. Evaporation of the fuel from the fuel container can be seen in Movie S6, Supporting Information.

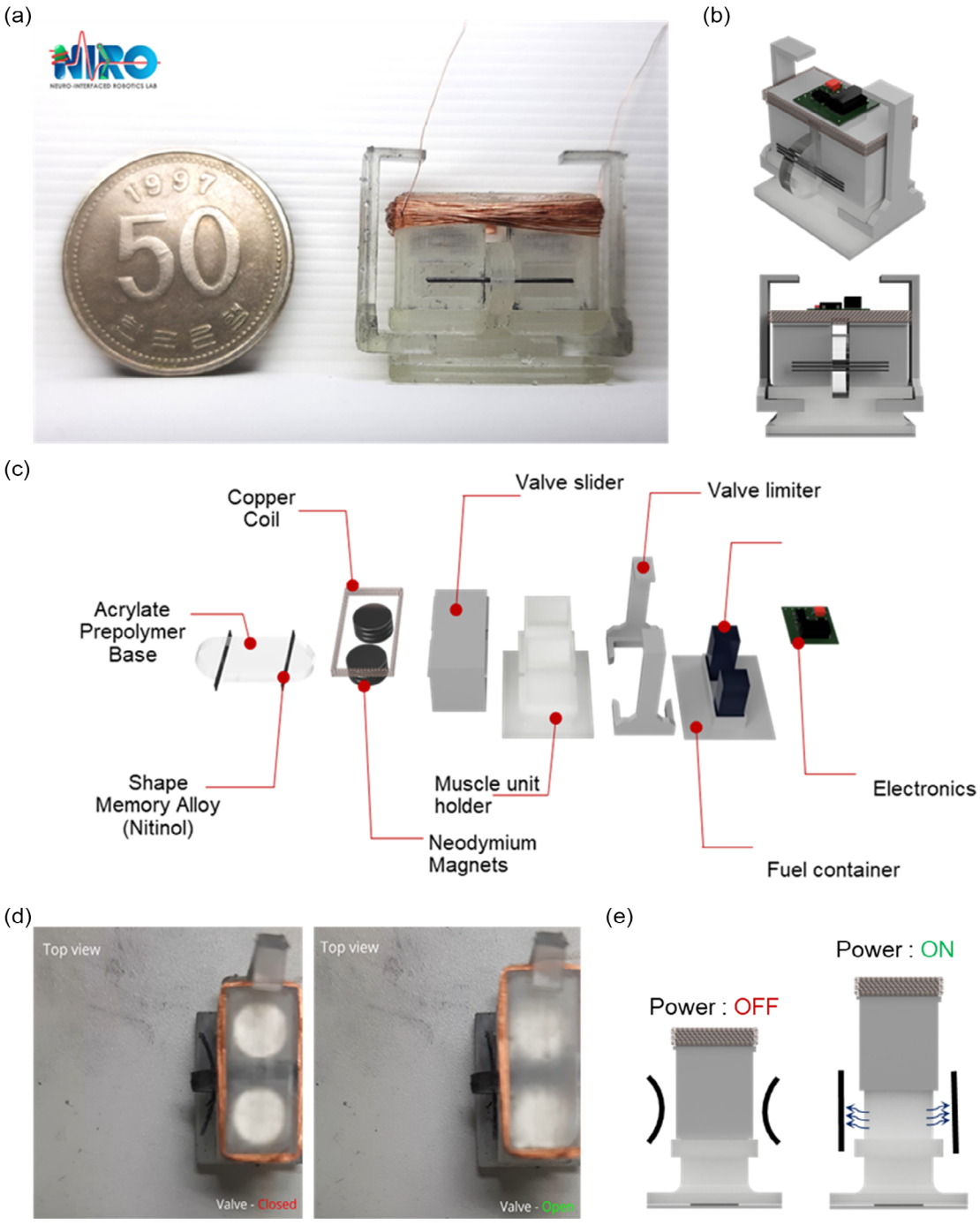

Figure 6. a) Photograph of biomimetic modular artificial muscle (BiMAM) next to a coin for size scaling. b) The 3D conceptual model of BiMAM. c) Exploded view of BiMAM. d) The basic operation of BiMAM. e) Graphically illustrated operational concept of BiMAM. Moreover, since the fuel-valve system can be operated using a microcontroller board, it can take inputs from any sensor and allow for programming a trigger-based actuation.

In our experience, if the catalytic-coated SMA actuator was not in operation for a long period (after being in operation at least once), the Pt black nanoparticles lose their ability to catalytically react and heat the SMA actuator wire. This coincides with the phenomenon observed by Applegate J., where the author reported that when the catalytic nanoparticles were not in operation for a long period of time (>24 h), the reactive activity of the catalytic nanoparticles had diminished.[41] To counteract this limitation, we introduced modularity in designing BiMAM. This allows the AMU to be removed and replaced from BiMAM easily in case there is poisoning or blockage of active sites on the catalytic coating of the SMA wires. Figure S17,

Supporting Information, shows how the AMU can be removed from the BiMAM for replacement.

The electromagnetic valve system is capable of superfast operation. Movie S7, Supporting Information, shows the different speeds at which the valve system can operate. The basic working of the electromagnetic valve system and the AMU is shown in Figure 6d and is schematically represented in Figure 6e. When the coil is energized, the repulsive electromagnetic force is generated against the neodymium magnets, which pushes the sliding valve up and exposes the methanol fumes to the AMU. Upon de-energizing the coil, the valve shuts off and cutting off the methanol fume contact and pausing the catalytic heating. An Arduino UNO development board is used to power and operate the valve, with basic codes written on Arduino IDE software. This type of electric control allows the fuel-valve system to work at high frequencies up to 1000 Hz. This characteristic can help achieve temperature control of catalytic heating on the surface of the catalyst-coated NiTi wire. With the inclusion of a feedback system, it is possible to open and close the valve at certain frequencies to control the methanol fume contact with the catalyst-coated target. Using this method, overheating of AMU can be avoided and a stable continuous actuation can be achieved.

We demonstrated this by using an EMG sensor (Sparkfun's Myoware Muscle Sensor) input to trigger the opening of the valve in BiMAM. Figure S18, Supporting Information, shows the flowchart to depict this use case. As seen in Movie S8, Supporting Information, when the user flexes the muscle, the EMG sensor sends a signal that is read by the microcontroller board and the

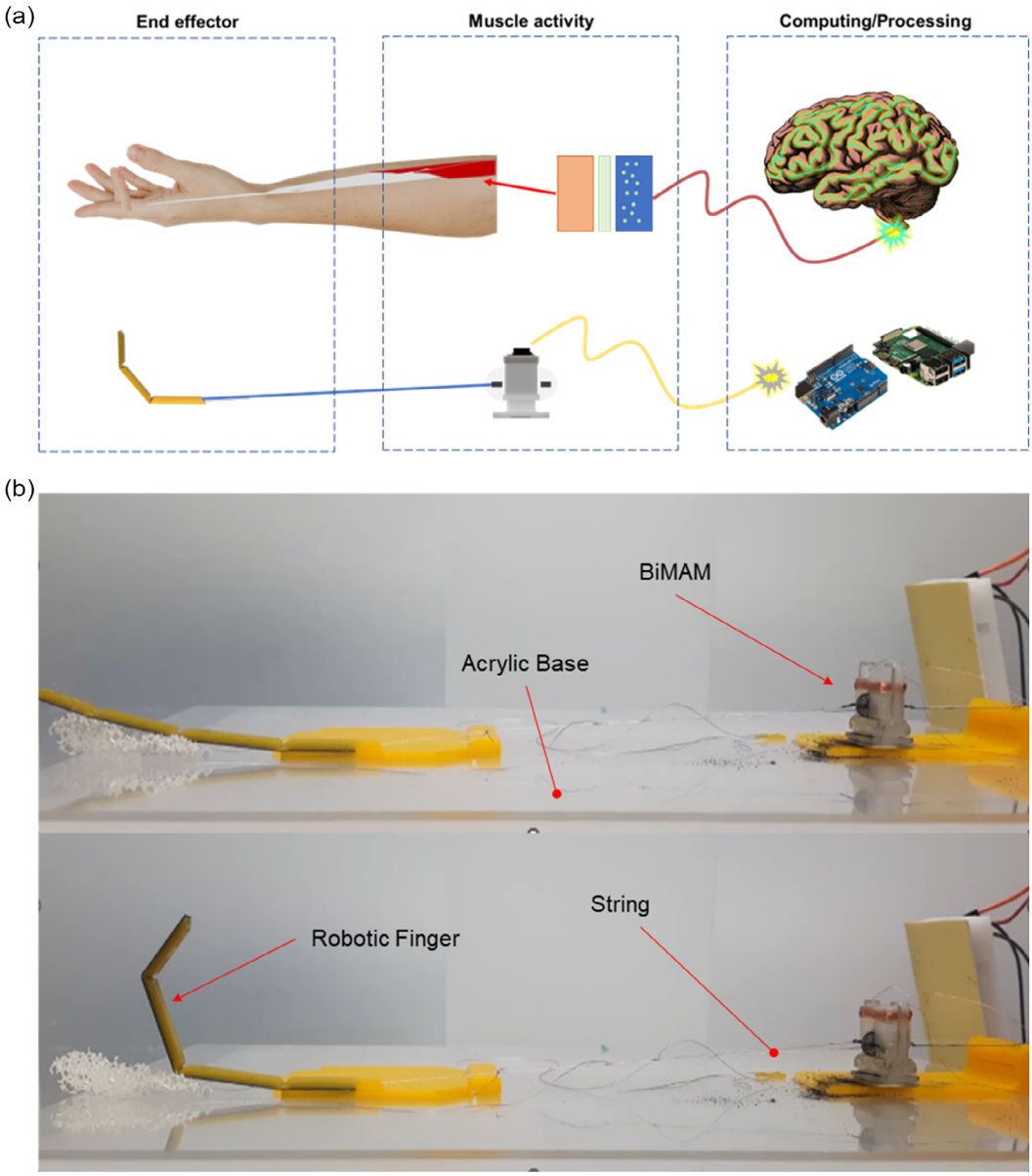

Figure 7. a) A straightforward comparison between the conceptual sequential process of moving a finger (top) and moving a robotic finger (bottom). b) Experimental setup of the robotic finger curling using BiMAM.

pre-programmed microcontroller delivers an output signal that energizes the coil which results in the opening of the valve system. This experiment shows the potential of BiMAM to be controlled by any commercially available development boards and sensor modules.

Figure 7a shows the conceptual idea behind the development of BiMAM. Figure 7b shows the entire experimental setup that mimics the sequence of the skeletal muscle actuation process. The robotic finger is fabricated using a 3D printer (160M Moment 3D Printer). The material used is PLA. The finger is divided into four segments, each containing a slot for a string to pass through. This string is bonded only to the tip of the finger and passes freely through the slots of the other segments. The other end of this string is used for coupling it with BiMAM. The AMU in this particular module uses 375 μm diameter NiTi wires. Both the tips of the NiTi wires are also bonded with strings using a strong adhesive. These cotton strings essentially behave like the actin element in a skeletal muscle (but in this case are permanently bonded to the myosin element and do not release). The string from one side of the BiMAM is connected to the string of the robotic finger. The other side string is attached to a holder which is fixed on an acrylic base. Upon receiving an electrical trigger from the computer, BiMAM actuates. The stroke length and the pull force produced by BiMAM are sufficient to move the finger as seen in Movie S9, Supporting Information.

The time taken to curl the robotic finger by BiMAM is longer than anticipated. We hypothesize that the observed discrepancies between the speed of actuation of AMU in Section 2.2 and the speed of curling robotic fingers can associate with factors like external disturbances, insufficient fume concentration, and mechanical interruption.

Noticeably, the overall length of BiMAM used to move the robotic finger is less than 20 mm. The total wire length used in this demonstration of BiMAM was 24 mm. In comparison, if the NiTi wire was used in the conventional straight configuration, a 100 mm long NiTi wire will be required to produce the same movement in the robotic finger. This validates the fact that an unconventional biomimetic design of SMA can provide larger strokes at the centimeter scale that can be further utilized in robotic and bionic applications.

3. Conclusion

In this article, we introduced BiMAM, a chemically powered modular artificial muscle capable of electronic manipulation. This modular design combines CNT/Pt-hybrid SMA wires and a centimeter-scale electromechanical unit for fuel storage and delivery. The main advantage of BiMAM is its ability to electronically control a chemically powered SMA actuator, with all the driving elements, including electronic components, fuel storage, and the fuel-control valve, integrated into the module. BiMAM also requires four times less electric current to initiate actuation compared to Joule heating–driven SMA actuator. The module can be controlled through any microcontroller and programmed to respond to various inputs, such as EMG signal input, or digital/analog sensors, while being powered by chemical energy. Additionally, the biomimetic design of the AMU allows for larger strokes than conventional linear strokes in SMA actuation.

The innovations that made the development of BiMAM possible can be categorized into two parts: the fabrication of the CNT/Pt-hybrid SMA with a flexible AMU and the prototyping of an electromagnetic-based centimeter-scaled valve system. Testing of catalytic combustion-based heating of AMU using methanol was conducted to characterize the effect of distance between the fuel source and catalyst-coated target. The performance of a single-wired AMU demonstrated pull forces between 0.3 and 0.6 N, achieving a stroke length of 15%–25% of the wire length. No-load actuation speeds up to 0.5 s were recorded along with 4.5 s of cooling (relaxation) time when subjected to a counteracting spring-bias force. A working frequency of 0.18 Hz was achieved, and AMU demonstrated over 100+ cycles with an average stroke of 2 mm for more than 10 min. The electromagnet-based valve system of our modular artificial muscle showed working frequencies of up to 1000 Hz. The coil system in our module uses four times less current compared to Joule heating for actuating the 250 μm thin wire. We also demonstrated the activation of the electromagnet-based valve system based on muscle movements from a human hand using a surface EMG sensor. Lastly, we showcased the application of BiMAM by demonstrating the curling movement of a robotic finger.

This work presents an innovative approach toward designing an electronically controllable fuel-based artificial muscle by developing a solution that provides onboard fuel delivery using an electromechanical valve system combined with catalytic heating of the AMU. Furthermore, the utilization of adjusting-curve actuation of SMA, inspired by the myosin element in the skeletal muscle, demonstrates competitive performance in terms of actuation stroke length and speed compared to previous similar works. Moreover, by demonstrating EMG control and robotic finger actuation, this work represents the first step toward showcasing the potential for developing chemically powered bionics for humans. Future research can explore different actuating and catalytic materials, chemical fuels, and design strategies.

4. Experimental Section

Software—Autodesk Fusion 360: Fusion 360, an open-source 3D design software by Autodesk, was used to model the SMA wire to estimate the achievable stroke lengths at different bending diameters. The information about outer-surface strain values and the corresponding bending diameter ratios were occupied by a manufacturer. Based on our requirements of actuating force values in our configuration, we decided to model and estimate stroke lengths for 10 and 12 mm long SMA wires of 0.25 mm thickness. Using the bend diameter ratios for the outer-surface strain values up to 8%, we produced different models to measure the achievable stroke length upon actuation. The total stroke length in our configuration would be the displacement of the tip from the bent state (deformed state) to the straight state (actuated state). Although obvious, it was important to note that outer-surface strain values beyond 4% did not produce any useful stroke since the bending diameter was too small and the tips of the SMA wire started bending inward. Moreover, outer-surface strain values beyond 4% could cause permanent damage to the NiTi wire. The molds, supports, and modules used in this work were designed using the same 3D modeling software.

The Fabrication Process of the Artificial Muscle Unit: Acrylate prepolymer was used as a base for holding the SMA wires in place. Molds A and B are 3D designed, 3D modeled on Fusion 360 software, and printed using a 3D

printer (M160 Moment 3D printer) with PLA as the material. Additionally, they were designed with the purpose of using them repeatedly for fabricating multiple units of artificial muscle. A thin plastic film was placed on Mold A. Based on the stress generation requirement, several NiTi wires could be inserted in Mold A through the plastic film. The pattern of placing the NiTi wire was also subject to the use case. After that, Mold B was placed over the top of Mold A. Elastic bands were used to keep Mold B from moving and tightly in contact with Mold A. To act as a base for holding the NiTi wires in place, acrylate prepolymer was used in the development. Once acrylate polymer was poured into mold B, it was set for ultraviolet curing to harden up. UV curing was carried out for 12 min, with 405 nm as the wavelength of the UV light. After curing, the molds were taken apart and the fabricated muscle unit was taken out. The plastic films could be removed from the molds and the molds could be reused for fabricating more muscle units. The process of coating SMA wires was done using the dip-coating method. The NiTi wires are subjected to abrasion to form a rough surface. This is done to enhance the CNT attachment onto the wire. CNT is attached to the abrased NiTi wire by the dip-coating method. The solution for dip-coating comprised isopropyl alcohol (IPA, 100 mL). After every dip of NiTi wire in the CNT/IPA solution, it was briefly heated to 50 °C using a heat gun. This was done so that the IPA solvent quickly evaporated, leaving the CNT wires on the NiTi wire surface. This process of dipping and heating was done till a uniform layer of CNT coat is formed on the wire. To achieve the same thickness every time, the layering process was observed under a microscope (Olympus BX53 Semi-Motorized Fluorescence Microscope). For attaching Pt black over the CNT coating, a similar method to dip-coating was used. Pt black was mixed with acetone to form a sludge-like texture. The CNT-coated wire was driven through this sludge and heat blown by the heat gun after every dip. This way acetone evaporated rapidly leaving Pt black on the CNT-coated NiTi wire. Moreover, excess Pt black was blown out using a heat gun, resulting in no loose particles on the surface.

Experimental Setup for Distance-Effect between Methanol Source and Catalyst-Coated Sensor: A K-type thermocouple was coated with the same method that was used for coating the NiTi wire to perform catalytic heating on its surface. During the experiment, the K-type thermocouple sensor was suspended on top of a methanol fuel source container at a distance of 2, 4, and 6 mm respectively. This container had a volume of 1 cm^3 and the top of this container had a sliding valve flap which was attached to a servomotor. This servomotor was essentially used for opening and closing the flap over the methanol fuel container to control the exit of fumes from the container, acting as a valve system. When this valve was in the open state, the methanol fumes were free to diffuse in the air and contact the K-type thermocouple sensor suspended over it. The servo was controlled with an Arduino Uno microcontroller development board. The temperature limits were set as per the actuation requirements of the SMA wires. The temperature limits were set as 90 and 40 °C corresponding to the heating (actuating) and cooling (relaxing) temperatures of SMA, respectively. When the sensor temperature reading was below 40 °C, the valve system switched to open state. The temperature reading started rising and when the temperature reading exceeded 90 °C, the valve switched to the closed state. This cut off the fume contact with the sensor and the temperature started decreasing. The cycle of heating and cooling continued and kept the valve system automated.

Experimental Setup for 6 mm Distance-Effect on SMA Actuation: AMU was suspended on top of a methanol fuel source container at a distance of 6 mm. This container had a volume of 1 cm^3 and the top of this container had a sliding valve flap which was attached to a servomotor. This servomotor was essentially used for opening and closing the flap over the methanol fuel container to control the exit of fumes from the container, acting as a valve system. When this valve was in the open state, the methanol fumes were free to diffuse in the air and contact with AMU suspended over it. The experiment was carried out with the four open-state valve timings—1, 2, 4, and 6 s.

Experimental Setup for Speed of SMA Actuation: AMU was suspended on top of a methanol fuel source container at a distance of 2 mm. This container had a volume of 1 cm^3 and the top of this container had a sliding valve flap which was attached to a servomotor. This servomotor was essentially used for opening and closing the flap over the methanol fuel container to control the exit of fumes from the container, acting as a valve system. When this valve was in the open state, the methanol fumes were free to diffuse in the air and contact with AMU suspended over it. The servomotor was programmed to open and close the flap for the desired time window using an Arduino Uno Development board. A total of 9 time windows were tested. The duration of the time windows were as follows—0.1, 0.2, 0.3, 0.4, 0.5, 0.6, 0.7, 0.8, and 0.9 s.

Materials: The materials used were FLEXINOL NiTi9 wires (Dynalloy, Inc.), platinum nanoparticles (platinum black HiSPEC 1000, Alfa Aesar), short-MWCNTs nanowires (Sigma Aldrich), methanol (99.8% purity, Sigma Aldrich), isopropyl alcohol (99.5% purity, Sigma Aldrich), clear resin (Formlabs), and acrylate prepolymer (caprolactone tris (2-hydroxyethyl) isocyanurate triacrylate, 1,6-hexanediol diacrylate, and (1-hydroxycyclohexyl) phenylmethanone).

Supporting Information

Supporting Information is available from the Wiley Online Library or from the author.

Acknowledgements

This research was supported by a Korea Medical Device Development Fund grant funded by the Korea government (the Ministry of Science and ICT, the Ministry of Trade, Industry and Energy, the Ministry of Health & Welfare, the Ministry of Food and Drug Safety) (Project number: 1711174475, KMDF_PR_20200901_0158)

Conflict of Interest

The authors declare no conflict of interest.

Data Availability Statement

The data that support the findings of this study are available in the supplementary material of this article.

Keywords

biomimetic, chemical actuation, modular artificial muscle, shape memory alloy

Received: April 19, 2023
Revised: June 10, 2023
Published online: July 25, 2023

[1] C. Gotti, A. Sensini, A. Zucchelli, R. Carloni, M. L. Focarete, *Appl. Mater. Today* **2020**, *20*, 100772.
[2] Y. Gao, C. Zhang, *Smart Mater. Struct.* **2015**, *24*, 033002.
[3] E. Kim, Y. Jang, H. Kim, D. Y. Lee, J. G. Choi, S. J. Kim, *Sens. Actuators B Chem.* **2022**, *371*, 132556.
[4] C. Laschi, B. Mazzolai, M. Cianchetti, *Sci. Robot* **2016**, *1*, eaah3690.
[5] Y. Cui, D. Li, C. Gong, C. Chang, *ACS Nano* **2021**, *15*, 13712.
[6] H. Wang, P. York, Y. Chen, S. Russo, T. Ranzani, C. Walsh, R. J. Wood, *Int. J. Rob. Res.* **2021**, *40*, 895.
[7] Q. He, Z. Wang, Z. Song, S. Cai, *Adv. Mater. Technol.* **2019**, *4*, 1800244.
[8] P. Rothemund, N. Kellaris, S. K. Mitchell, E. Acome, C. Keplinger, *Adv. Mater.* **2021**, *33*, 2003375.

[9] Y. Jang, S. M. Kim, E. Kim, D. Y. Lee, T. M. Kang, S. J. Kim, *Microsyst. Nanoeng.* **2021**, *7*, 70.
[10] Y. Wang, C. Liu, L. Ren, L. Ren, *Biodes. Manuf.* **2022**, *5*, 174.
[11] P. Nagwade, *Int. J. Adv. Sci. Eng. Technol.* **2018**, *6*, 19.
[12] M. Shi, E. M. Yeatman, *Microsyst. Nanoeng.* **2021**, *7*, 95.
[13] Z. S. Davidson, H. Shahsavan, A. Aghakhani, Y. Guo, L. Hines, Y. Xia, S. Yang, M. Sitti, *Sci. Adv.* **2023**, *5*, eaay0855.
[14] P. Yuan, J. M. McCracken, D. E. Gross, P. V. Braun, J. S. Moore, R. G. Nuzzo, *Soft Matter* **2017**, *13*, 7312.
[15] L. Hines, K. Petersen, G. Z. Lum, M. Sitti, *Adv. Mater.* **2017**, *29*, 1603483.
[16] R. H. Baughman, *Science* **2005**, *308*, 63.
[17] E. Acome, S. K. Mitchell, T. G. Morrissey, M. B. Emmett, C. Benjamin, M. King, M. Radakovitz, C. Keplinger, *Science* **2018**, *359*, 61.
[18] X. Xie, L. Qu, C. Zhou, Y. Li, J. Zhu, H. Bai, G. Shi, L. Dai, *ACS Nano* **2010**, *4*, 6050.
[19] Q. Pei, M. Rosenthal, S. Stanford, H. Prahlad, R. Pelrine, *Smart Mater. Struct.* **2004**, *13*, N86.
[20] I. Boblan, A. Schulz, in *ISR 2010 (41st Int. Symp. on Robotics) and ROBOTIK 2010 (6th German Conf. on Robotics)*, Munich, Germany **2010**, pp. 1–6.
[21] J. Li, G. Zhong, H. Yin, M. He, Y. Tan, Z. Li, in *IEEE Int. Conf. on Robotics and Automation (ICRA)*, IEEE, Piscataway, NJ **2017**, pp. 4941–4946.
[22] J. Zhang, J. Sheng, C. T. O'Neill, C. J. Walsh, R. J. Wood, J.-H. Ryu, J. P. Desai, M. C. Yip, *IEEE Trans. Robot.* **2019**, *35*, 761.
[23] M. S. Kalairaj, H. Banerjee, C. M. Lim, P.-Y. Chen, H. Ren, *RSC Adv.* **2019**, *9*, 34244.
[24] V. H. Ebron, Z. Yang, D. J. Seyer, M. E. Kozlov, J. Oh, H. Xie, J. Razal, L. J. Hall, J. P. Ferraris, A. G. MacDiarmid, R. H. Baughman, *Science* **2006**, *311*, 1580.
[25] X. Yang, L. Chang, N. O. Pérez-Arancibia, *Sci. Robot* **2020**, *5*, eaba0015.
[26] F. Maimani, A. A. Calderón, X. Yang, A. Rigo, J. Z. Ge, N. O. Pérez-Arancibia, *Sens. Actuators A Phys.* **2022**, *341*, 112818.
[27] S. Kim, C. Laschi, B. Trimmer, *Trends Biotechnol.* **2013**, *31*, 287.
[28] M. Kruusmaa, P. Fiorini, W. Megill, M. de Vittorio, O. Akanyeti, F. Visentin, L. Chambers, H. El Daou, M.-C. Fiazza, J. Ježov, M. Listak, L. Rossi, T. Salumae, G. Toming, R. Venturelli, D. S. Jung, J. Brown, F. Rizzi, A. Qualtieri, J. L. Maud, A. Liszewski, *IEEE Robot. Autom. Mag.* **2014**, *21*, 51.
[29] H. Lu, M. Zhang, Y. Yang, Q. Huang, T. Fukuda, Z. Wang, Y. Shen, *Nat. Commun.* **2018**, *9*, 3944.
[30] M. Calisti, M. Giorelli, G. Levy, B. Mazzolai, B. Hochner, C. Laschi, P. Dario, *Bioinspir. Biomim.* **2011**, *6*, 036002.
[31] S. Coyle, C. Majidi, P. LeDuc, K. J. Hsia, *Extreme Mech. Lett.* **2018**, *22*, 51.
[32] D. Yun, *J. Mech. Sci. Technol.* **2018**, *32*, 1787.
[33] I. H. Kim, S. Choi, J. Lee, J. Jung, J. Yeo, J. T. Kim, S. Ryu, S. Ahn, J. Kang, P. Poulin, S. O. Kim, *Nat. Nanotechnol.* **2022**, *17*, 1198.
[34] *Surface Strains in Nitinol Wire, Ribbon and Sheet*, Johnson Matthey, London, UK, https://matthey.com/products-and-markets/other-markets/medical-components/resource-library/surface-strains-in-nitinol-wire-ribbon-and-sheet.
[35] H.-T. Lee, F. Seichepine, G.-Z. Yang, *Adv. Funct. Mater.* **2020**, *30*, 2002510.
[36] Jianwei Che, Tahir Çagin, W. A. Goddard III, *Nanotechnology* **2000**, *11*, 65.
[37] Y. Tadesse, A. Villanueva, C. Haines, D. Novitski, R. Baughman, S. Priya, *Smart Mater. Struct.* **2012**, *21*, 045013.
[38] J. G. Park, Q. Cheng, J. Lu, J. Bao, Y. Tian, R. Liang, B. Wang, C. Zhang, J. S. Brooks, in *18th Int. Conf. on Composite Materials*, Jeju Island, South Korea **2011**.
[39] Z. Hu, V. Boiadjiev, T. Thundat, *Energy Fuels* **2005**, *19*, 855.
[40] S. Pham, Y. Puckett, in StatPearls, Treasure Island, **2023**, https://www.ncbi.nlm.nih.gov/books/NBK559006/.
[41] J. R. Applegate, D. McNally, H. Pearlman, S. D. Bakrania, *Energy Fuels* **2013**, *27*, 4014.